

# PERCEPTION THROUGH 2D-MIMO FMCW AUTOMOTIVE RADAR UNDER ADVERSE WEATHER

Xiangyu Gao, Sumit Roy, Guanbin Xing, Sian Jin

{xygao, sroy, gxing, sianjin} @uw.edu

Dept. of Electrical and Computer Engineering, University of Washington

## ABSTRACT

Millimeter-wave (mmWave) radars are being increasingly integrated in commercial vehicles to support new Adaptive Driver Assisted Systems (ADAS) features that require accurate location, velocity, and angle estimates of objects, largely independent of environmental conditions. To explore radar-based ADAS applications, we have updated our frequency-modulated continuous wave (FMCW) radar test-bed with Texas Instrument's (TI) 4-chip cascaded radar that forms large 2D MIMO virtual array. In this paper, we develop the necessary received signal models for applying different direction of arrival (DoA) estimation algorithms and experimentally validating their performance under controlled scenarios. To test the robustness of mmWave radars under adverse weather conditions, we collected raw radar data (I-Q samples post demodulated) dataset for various objects by a driven vehicle-mounted platform, specifically for snowy and foggy situations where cameras are largely ineffective. Initial results from radar imaging algorithms to this dataset are presented.

**Index Terms**— mmWave, FMCW, 2D MIMO, DoA, cascaded radar, sparse array, adverse weather, snow, ADAS.

## 1. INTRODUCTION

To meet the requirement for ADAS and especially L4/L5 autonomous driving [1], automotive radars need to have a high angular resolution. The angular resolution of a radar system can be enhanced with an increasing antenna aperture by synthesizing aperture along radar movement [2], forming virtual array via multiple-input and multiple-out (MIMO) technique [3], using more antenna elements, or creating a sparse array [4] with larger antenna distance.

With the received signals at array elements, the DoA of targets can be extracted by proper signal processing. The FFT-based DoA method and the multiple signal classification (MUSIC) are discussed and experimented in [5] on a 2 TX and 4 RX MIMO virtual array. Particularly for a sparse array, the compressive sensing (CS) methods have been exploited in DoA estimation to reconstruct the missing antenna elements and mitigate the high side lobes [6, 7, 8]. The sparse condition

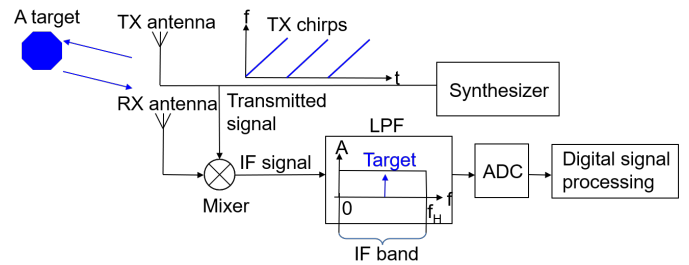


Fig. 1. Basic FMCW radar block diagram

is fulfilled in CS-based DoA estimation as a very small amount of targets is expected at each range-Doppler cell.

MmWave radar is well known for its excellent environmental resistance and robustness under adverse weather conditions [9], while there has been little published work to date experimentally verifying this hypothesis due to the difficulty of capturing data in such circumstances. Prior work [10] studied the effect of fog on the mmWave propagation, and Gao et al. [11] showed a robust and high-performance object recognition algorithm verified at nighttime where cameras are largely ineffective due to the low-light.

In this paper, we show a mmWave FMCW radar test-bed with the state-of-art TI high-resolution (2D array) radar [12], and a radar dataset collected under different adverse weathers (snow, fog) using this test-bed. Several experiments have been done with our test-bed and dataset to present some preliminary results that validate its capabilities in terms of DoA estimation and environment imaging.

## 2. FMCW MIMO RADAR

### 2.1. FMCW Radar and Range Estimation

The FMCW radar transmits periodic wide-band linear frequency-modulated signal (called chirps) as shown in Fig. 1. The transmit (TX) signal is reflected by targets and received at the radar receiver. FMCW radars can detect targets' range and velocity from the received (RX) signal using the stretch or de-chirping processing structure [5] in Fig. 1.

In this structure, a mixer at the receiver multiplies the RX signal with the TX signal to produce an intermediate fre-

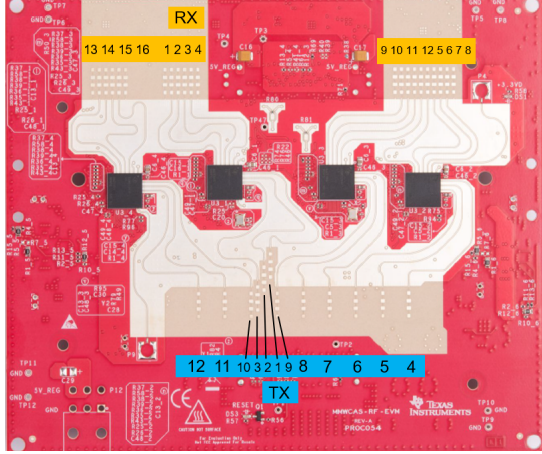


**Fig. 2.** Texas Instrument 4-chip cascaded radar board [12] and the position of antennas.

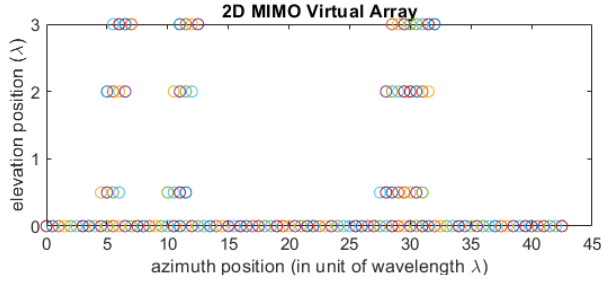


**Fig. 3.** 2D MIMO virtual array formed by 12 TX and 16 RX.

quency (IF) signal. Since the RX signal and the TX signal are linear frequency modulated signal that has constant frequency difference determined by target's location, the IF signal is a single-tone signal. For example, the IF signal for a target at range  $r$  has frequency  $f_{IF} = \frac{2r}{c} S$ , the multiplication of round-trip delay  $\frac{2r}{c}$  with chirp slope  $S$ , where  $c$  denotes the speed of the light. Thus, detecting the frequency of the IF signal can solve the target range. At the end of receiver, IF signal is passed into an anti-aliasing low-pass filter (LPF) and an analog-to-digital converter (ADC) for following digital signal processing. A fast Fourier transform (FFT) is widely adopted to estimate  $f_{IF}$  to infer  $r$ , and hence such operation is called the *Range FFT*.

## 2.2. MIMO Virtual Array

To estimate the angle of targets, a receive antenna array is needed. In MIMO radar, TX antennas transmit orthogonal chirp sequence, which enables the contribution of each TX can be extracted at each RX antenna [13]. That is, if a MIMO radar has  $M_T$  TX antennas and  $M_R$  RX antennas with appropriate arrangement, a virtual array with  $M_T M_R$  elements can be synthesized [3]. The virtual array steering vectors are equivalent to the steering vectors result from a spatial convolution of the

transmit and receive phase centers [14].

In this paper, a 4-chip cascaded mmWave radar board [12] from TI is adopted for experiments. This cascaded radar includes 12 TX antennas and 16 RX antennas placed in the 2D manner shown in Fig. 2, which would create a sparse 2D virtual array (Fig. 3) with 192 elements in total. The virtual array in bottom horizontal direction is a dense uniform linear array with 86 elements, and the antennas in vertical direction form the minimum redundancy array [4] with equivalent aperture achieved by 7 elements (i.e., element spacing  $\lambda/2$ ).

## 3. SYSTEM MODEL FOR DOA ESTIMATION

Without loss of generality, we model a 2D uniform plane array (UPA) arranged in the vertical plane with  $M$  antenna elements in each row and  $N$  antenna elements in each column (shown in Fig. 4). The array response is given by [15]:

$$\mathbf{y} = \mathbf{A}\mathbf{s} + \mathbf{n} \quad (1)$$

where  $\mathbf{A} = [\mathbf{a}_1, \dots, \mathbf{a}_K]$  is the array steering matrix for  $K$  targets with

$$\mathbf{a}_k = \mathbf{a}(\phi_k) \otimes \mathbf{a}(\theta_k)$$

$$\mathbf{a}(\phi_k) = \left[ 1, e^{j(2\pi/\lambda)d \sin(\phi_k)}, \dots, e^{j(2\pi/\lambda)(M-1)d \sin(\phi_k)} \right]^T$$

$$\mathbf{a}(\theta_k) = \left[ 1, e^{j(2\pi/\lambda)d \sin(\theta_k)}, \dots, e^{j(2\pi/\lambda)(N-1)d \sin(\theta_k)} \right]^T$$

Here,  $\mathbf{a}(\phi_k)$  and  $\mathbf{a}(\theta_k)$  are steering vectors for elevation angle  $\phi_k$  and azimuth angle  $\theta_k$  for  $k$ th target, respectively.  $\otimes$  denotes the Kronecker product operation.  $\mathbf{n}$  is a noise term, and  $\mathbf{s} = [\beta_1, \dots, \beta_K]^T$ , where  $\beta_k$  denotes the reflection coefficient for the  $k$ th target.

For a 1D linear array, angle finding can be done with digital beamforming (DBF) by performing FFT across the array elements [5]. This FFT-based method can be extended to above 2D UPA, i.e., perform first FFT on the horizontal elements and second FFT on the elevation elements. DBF is *computationally efficient* but is not a high-resolution method.

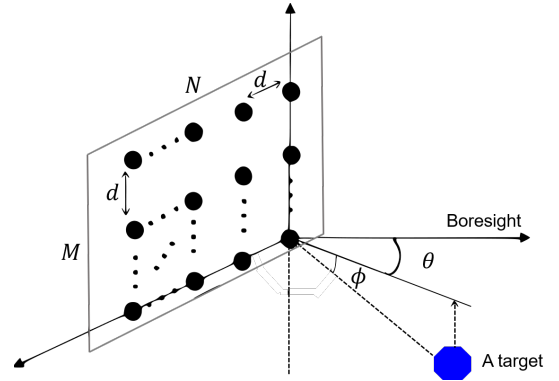


**Fig. 4.** System model of uniform plane array.

**Table 1.** Parameter calculation (based on [5]) and configuration for 4-chip cascaded radar test-bed

Parameter	Calculation Equation	Configuration	Value
Range resolution ( $R_{\text{res}}$ )	$R_{\text{res}} = \frac{c}{2B} = 0.39 \text{ m}$	Frequency ( $f_c$ )	77 GHz
Velocity resolution ( $V_{\text{res}}$ )	$V_{\text{res}} = \frac{\lambda}{2N_c T_c} = 0.0631 \text{ m/s}$	Sweep Bandwidth ( $B$ )	384 MHz
Azimuth Angle resolution ( $\theta_{\text{res}}$ ) <sup>1</sup>	$\theta_{\text{res}} = \frac{\lambda}{L_n \cos \theta} \approx 1.35^\circ$	Sweep slope ( $S$ )	45 MHz/ $\mu\text{s}$
Elevation Angle resolution ( $\phi_{\text{res}}$ ) <sup>2</sup>	$\phi_{\text{res}} = \frac{\lambda}{L_v \cos \theta} \approx 19^\circ$	Sampling frequency ( $f_s$ )	15 Msps
Max operating range ( $R_{\text{max}}$ )	$R_{\text{max}} = \frac{f_s c}{2S} = 50 \text{ m}$	Num of chirps in one frame ( $N_c$ )	128
Max operating velocity ( $V_{\text{max}}$ )	$V_{\text{max}} = \frac{\lambda}{4T_c} = 4.04 \text{ m/s}$	Num of samples of one chirp ( $N_s$ )	128
Max operating azimuth angle ( $\theta_{\text{max}}$ )	$\theta_{\text{max}} = \sin^{-1} \left( \frac{\lambda}{2d} \right) = 90^\circ$	Num of transmitters, receivers ( $M_T, M_R$ )	12, 16
Max operating elevation angle ( $\phi_{\text{max}}$ )	$\phi_{\text{max}} = \sin^{-1} \left( \frac{\lambda}{2d} \right) = 90^\circ$	Duration of chirp <sup>3</sup> and frame ( $T_c, T_f$ )	240 $\mu\text{s}$ , 33.3 ms

### 3.1. MUSIC

MUSIC belongs to the class of *eigen-decomposition* based DoA estimators that construct the  $(MN - K)$ -dimension noise subspace  $U_n$  and the left  $K$ -dimension signal subspace from the covariance matrix of received signals  $\mathbf{y}$  [16]. The azimuth and elevation angles  $(\theta_k, \phi_k)$  of the  $k$ th target can be found as peak on 2D MUSIC spectrum, which is given by

$$P_{\text{MUSIC}}(\theta_k, \phi_k) = \frac{1}{\mathbf{a}_k^H \mathbf{U}_n \mathbf{U}_n^H \mathbf{a}_k} \quad (2)$$

### 3.2. Compressive Sensing (CS)

To apply compressive sensing to DoA estimation, we need to define a search grid of  $K_g$  ( $K_g \gg K$ ) potential incident angles, and construct an hypothetical array steering matrix  $\tilde{\mathbf{A}} = [\mathbf{a}_1, \dots, \mathbf{a}_{K_g}]$  and the reflection coefficient matrix  $\tilde{\mathbf{s}} = [\beta_1, \dots, \beta_{K_g}]^T$ .

The compressive sensing DoA estimation problem can be solved by an  $\ell_1$ -norm optimization problem [17]:

$$\min \|\tilde{\mathbf{s}}\|_1 \quad \text{subject to} \quad \|\tilde{\mathbf{A}}\tilde{\mathbf{s}} - \mathbf{y}\|_2 \leq \epsilon \quad (3)$$

where  $\|\cdot\|_1$  is the  $\ell_1$ -norm forces the sparsity constraint, and  $\epsilon$  is a chosen upper bound for the reconstruction error. We perform the orthogonal matching pursuit (OMP) algorithm [18] to solve this problem.

## 4. EXPERIMENTS

### 4.1. Radar Test-bed and Configuration

We assembled a test-bed (see Fig. 5) of TI 4-chip cascaded radar [12] with extra binocular FLIR cameras (left and right).

<sup>1</sup> $\theta_{\text{res}}$  is determined by maximum horizontal aperture length  $L_h = 42.5\lambda$ .

<sup>2</sup> $\phi_{\text{res}}$  is determined by the maximum vertical aperture length  $L_v = 3\lambda$ .

<sup>3</sup> $T_c$  is equal to chirp interval times number of TX.

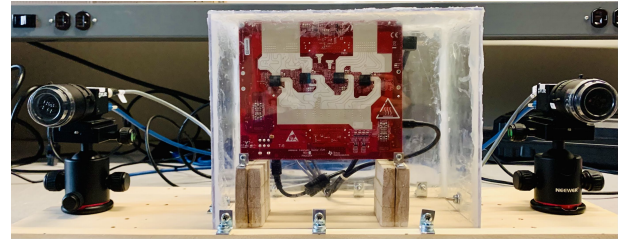


**Fig. 5.** 4-chip cascaded radar test-bed with 2 cameras.

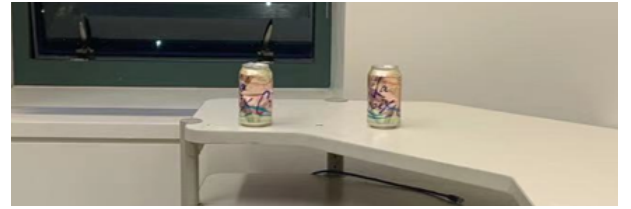


**Fig. 6.** Experiment setup with two targets separated by  $5^\circ$ .

Binocular cameras are synchronized with radar to provide the visualization for the imaging scenario. The 4-chip cascaded radar forms a 2D MIMO virtual array (see Fig. 3) via using time-division multiplexing (TDM) [3] on 12 TX antennas, which results in a larger amount of data to store ( $\sim 378 \text{ MB}$  raw data per second). Other parameters and configuration of this radar is set according to Table. 1.

### 4.2. DoA Estimation for Sparse Array

The 2D virtual array in Fig. 3 is mostly sparse, and we aim to evaluate the performance of different DoA estimators on it. We consider the experiment setup with two targets separated by  $5^\circ$  (see Fig. 6). Three DoA algorithms - FFT, MUSIC, and CS - are implemented on the received signal of the second-row elements of virtual array in Fig. 3. The estimated DoA spectrums are shown in Fig. 7, which demonstrate that the FFT and MUSIC behave worse than CS in the presence of a

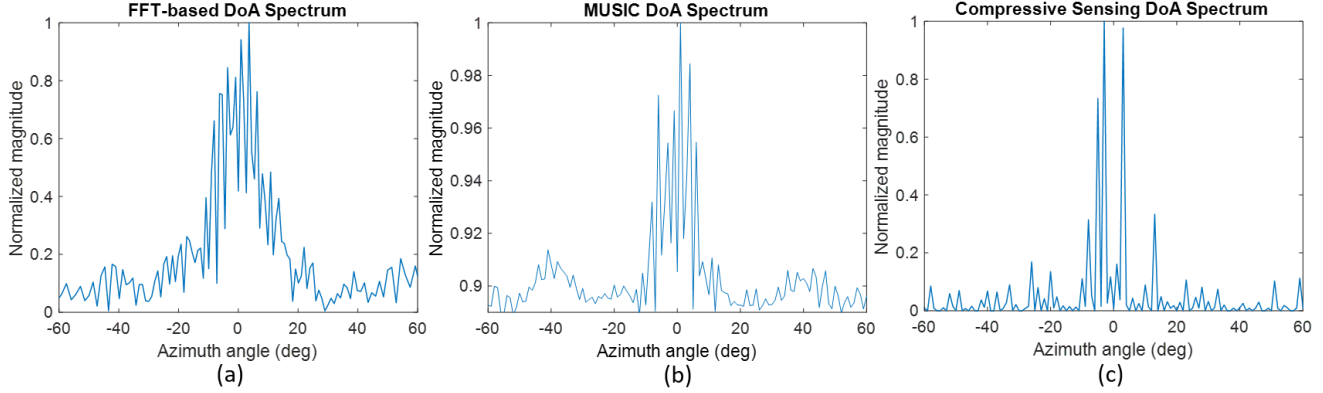


Fig. 7. DoA estimation results of the experiment in Fig. 6: (a) FFT-based method; (b) MUSIC; (c) Compressive Sensing.

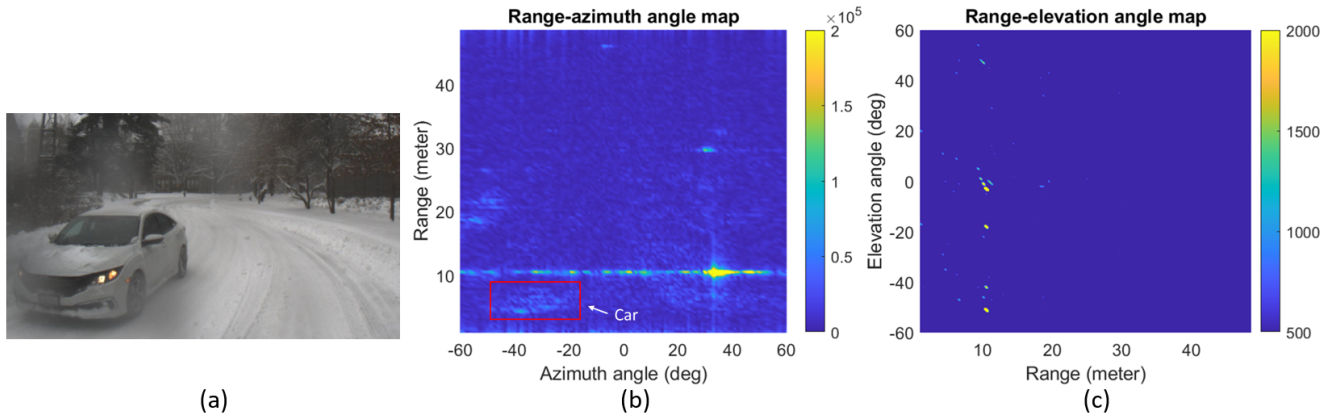


Fig. 8. Dataset example: (a) Camera image; (b) Range-azimuth angle map; (c) Range-elevation angle map.

high-sidelobe level characteristic of the sparse array.

### 4.3. Radar Dataset and Imaging for Adverse Weathers

For promoting the development of high-level radar ADAS applications (e.g., object recognition) under the critical adverse weathers, we mount the test-bed on a vehicle (see Fig. 9) and collect a raw radar I-Q samples dataset for various objects (pedestrian, cyclist, and car) by driving vehicle at the snowy and foggy situations where camera images are blurred.

We present one example from the collected dataset in



Fig. 9. Test-bed mounted on a vehicle for dataset collection.

Fig. 8, which corresponds to a slowly moving car. The raw data belongs to the bottom-row virtual array (Fig. 3) is processed with Range FFT and FFT-based DoA to generate a bird-view range-azimuth angle map (Fig. 8(b)), where the car is visible and highlighted. We also generate a range-elevation angle map by executing Range FFT and CS-based DoA on the raw data of one column of virtual array, and show it in Fig. 8(c).

## 5. CONCLUSION

In this paper, we show a mmWave FMCW radar test-bed with the state-of-art TI high-resolution (2D array) radar, and a radar dataset collected under different adverse weather (snow, fog) using this test-bed. Several experiments have been done on the test-bed and dataset to present some preliminary results that validate its capabilities in terms of DoA estimation and environment imaging.

## 6. REFERENCES

- [1] NHTSA, “Automated vehicles for safety,” <https://www.nhtsa.gov/technology-innovation/automated-vehicles-safety>.
- [2] X. Gao, S. Roy, and G. Xing, “Mimo-sar: A hierarchical high-resolution imaging algorithm for fmcw automotive radar,” 2021, Available at <https://arxiv.org/pdf/2101.09293.pdf>.
- [3] Sandeep Rao, *White paper: MIMO Radar*, Number SWRA554A. Texas Instrument, 2017, Available at <https://www.ti.com/lit/an/swra554a/swra554a.pdf>.
- [4] A. Moffet, “Minimum-redundancy linear arrays,” *IEEE Transactions on Antennas and Propagation*, vol. 16, no. 2, pp. 172–175, 1968.
- [5] X. Gao, G. Xing, S. Roy, and H. Liu, “Experiments with mmwave automotive radar test-bed,” in *2019 53rd Asilomar Conference on Signals, Systems, and Computers*, 2019, pp. 1–6.
- [6] F. Roos, P. Hügler, L. L. T. Torres, C. Knill, J. Schlichenmaier, C. Vasaneli, N. Appenrodt, J. Dickmann, and C. Waldschmidt, “Compressed sensing based single snapshot doa estimation for sparse mimo radar arrays,” in *2019 12th German Microwave Conference (GeMiC)*, 2019, pp. 75–78.
- [7] A. Correas-Serrano and M. A. González-Huici, “Experimental evaluation of compressive sensing for doa estimation in automotive radar,” in *2018 19th International Radar Symposium (IRS)*, 2018, pp. 1–10.
- [8] F. Roos, P. Hügler, J. Bechter, M. A. Razzaq, C. Knill, N. Appenrodt, J. Dickmann, and C. Waldschmidt, “Effort considerations of compressed sensing for automotive radar,” in *2019 IEEE Radio and Wireless Symposium (RWS)*, 2019, pp. 1–3.
- [9] Shizhe Zang, Ming Ding, D. Smith, P. Tyler, T. Rakotoarivelo, and Mohamed Ali Kâafar, “The impact of adverse weather conditions on autonomous vehicles: How rain, snow, fog, and hail affect the performance of a self-driving car,” *IEEE Vehicular Technology Magazine*, vol. 14, pp. 103–111, 2019.
- [10] Yosef Golovachev, Ariel Etinger, Gad Pinhasi, and Yosef Pinhasi, “Millimeter wave high resolution radar accuracy in fog conditions-theory and experimental verification,” *Sensors*, vol. 18, 07 2018.
- [11] X. Gao, G. Xing, S. Roy, and H. Liu, “Ramp-cnn: A novel neural network for enhanced automotive radar object recognition,” *IEEE Sensors Journal*, vol. 21, no. 4, pp. 5119–5132, 2021.
- [12] Texas Instrument, *White paper: Imaging Radar Using Cascaded mmWave Sensor Reference Design*, Number TIDUEN5A. Texas Instrument, 2019, Available at <https://www.ti.com/lit/ug/tiduen5a/tiduen5a.pdf>.
- [13] S. Sun, A. P. Petropulu, and H. V. Poor, “Mimo radar for advanced driver-assistance systems and autonomous driving: Advantages and challenges,” *IEEE Signal Processing Magazine*, vol. 37, no. 4, pp. 98–117, 2020.
- [14] F. C. Robey, S. Coutts, D. Weikle, J. C. McHarg, and K. Cuomo, “Mimo radar theory and experimental results,” in *Conference Record of the Thirty-Eighth Asilomar Conference on Signals, Systems and Computers, 2004.*, 2004, vol. 1, pp. 300–304 Vol.1.
- [15] K. Goto, T. Akao, K. Maruta, and C. Ahn, “Reduced complexity direction-of-arrival estimation for 2d planar massive arrays: A separation approach,” in *2018 18th International Symposium on Communications and Information Technologies (ISCIT)*, 2018, pp. 48–53.
- [16] R. Schmidt, “Multiple emitter location and signal parameter estimation,” *IEEE Transactions on Antennas and Propagation*, vol. 34, no. 3, pp. 276–280, 1986.
- [17] J. Ender, “A brief review of compressive sensing applied to radar,” in *2013 14th International Radar Symposium (IRS)*, 2013, vol. 1, pp. 3–16.
- [18] T. T. Cai and L. Wang, “Orthogonal matching pursuit for sparse signal recovery with noise,” *IEEE Transactions on Information Theory*, vol. 57, no. 7, pp. 4680–4688, 2011.